

Three-Body Earth-Moon Transfers with Different Departure/Arrival Orbital Altitudes: New Phenomenon and Diffusion Model-Augmented Construction

Shuyue Fu^{a,b}, Wenxuan Zhang^a, Di Wu^{a,d}, Shengping Gong^{a,c,*} and Peng Shi^{a,d}

^aSchool of Astronautics, Beihang University, Xueyuan Road No.37, 100191, Beijing, People's Republic of China

^bShen Yuan Honors College, Beihang University, Xueyuan Road No.37, Beijing, 100191, People's Republic of China

^cState Key Laboratory of High-Efficiency Reusable Aerospace Transportation Technology, 102206, Beijing, People's Republic of China

^dKey Laboratory of Spacecraft Design Optimization & Dynamic Simulation Technologies, Ministry of Education, 100191, Beijing, People's Republic of China

ARTICLE INFO

Keywords:

Planar restricted three-body problem
Bi-impulsive Earth-Moon transfer
Diffusion model
Grid search method

ABSTRACT

Construction of Earth-Moon transfers is the basis of missions to explore the Moon and cislunar space. The traditional grid search method suffers from a relatively low convergence rate and computational efficiency, mainly focusing on the distribution of transfer characteristic parameters. Moreover, when constructing transfers with different departure/arrival orbital altitudes, the process of grid search and trajectory correction should be repeated with a low convergence rate and computational efficiency. To address these limitations of the traditional grid search method, this paper is devoted to exploring an effective way to augment the grid search method. Bi-impulsive Earth-Moon transfers from a circular Earth parking orbit to a circular Moon target orbit in the Earth-Moon planar circular restricted three-body problem are considered in this paper. Firstly, the transfers are constructed, and the corresponding solution space is explored in terms of construction parameters, including departure phase angle at the Earth parking orbit, initial-to-circular velocity ratio, and time of flight. An interesting phenomenon about the discontinuous behavior of the time-of-flight distribution with respect to departure phase angle is identified. This phenomenon is further used to train a diffusion model, which aims to augment the traditional grid search method and generate high-quality initial guesses for transfers with different departure/arrival orbital altitudes. The construction results of the proposed method are presented and analyzed. The proposed diffusion model-augmented grid search method improves the convergence rate by 47.34-56.25% and saves the wall-clock time by 39.39-40.52% over the traditional grid search method relatively, while ensuring comparable transfer characteristics.

1. Introduction

Interest in the Earth-Moon transfers has been renewed due to the proposal of several missions to explore the Moon and cislunar space. For these missions, several transfer scenarios have been proposed, including the Earth-Moon transfers (transfers to circular Moon orbit [1–3] and multi-body periodic orbits around the Moon, such as distant retrograde orbit [4–6] and distant prograde orbit [7, 8]) and libration point transfers (transfers between/to periodic orbits of collinear libration points [9–11] and triangular libration points [12–14]). Among these scenarios, the bi-impulsive scenario from a circular Earth parking orbit to a circular Moon target orbit is a classical scenario for scholars to consider [1]. To construct such transfers, an appropriate dynamical model should be adopted. Several dynamical models have been adopted, including the patched two-body problem [15], the Earth-Moon planar three-body problem (PCR3BP) [16–18], the Sun-Earth/Moon planar bicircular restricted four-body problem (PBCR4BP) [1–3], and other higher-fidelity models [19–21]. Compared to transfers constructed in the patched two-body problem [15], there is a potential

*Corresponding author

✉ fushuyue@buaa.edu.cn (S. Fu); zwx03511@buaa.edu.cn (W. Zhang); wudi2025@buaa.edu.cn (D. Wu); gongsp@buaa.edu.cn (S. Gong); shipeng@buaa.edu.cn (P. Shi)

ORCID(s): 0009-0001-5111-9779 (S. Fu)

to use the multi-body problems (e.g., the Earth-Moon PCR3BP and the Sun-Earth/Moon PBCR4BP) to obtain more transfer families, including direct and low-energy transfers, to satisfy specific mission requirements. Therefore, to investigate more transfer families and further explore the solution space of bi-impulsive Earth-Moon transfers, one of the multi-body problems, i.e., the Earth-Moon PCR3BP, is adopted as the dynamical model to construct transfer trajectories.

Because there is no closed-form solution in the Earth-Moon PCR3BP, numerical methods are adopted to construct bi-impulsive transfers. Typically, the construction method can be divided into two steps: generation of initial guesses and trajectory correction. Firstly, the initial guesses of transfer trajectories are generated by several methods, including grid search [1, 3] and methods based on the dynamical structures [19, 22–24]. Then, initial guesses are corrected to satisfy the specific constraints, i.e., the departure/arrival orbital altitudes and tangential departure/arrival [1]. When adopting the methods based on the dynamical structures, invariant manifolds [22], weak stability boundary structures [19, 25], sequences of lobe dynamics [24], and other dynamical structures using multi-body prior knowledge [2, 26] are usually used. These methods can effectively obtain low-energy transfers, but suffer from a limited number of obtained solutions [27]. In contrast, the grid search method performs an exhaustive search of construction parameters and obtains feasible solutions using trajectory correction. This type of method typically yields more solutions and provides a global map to analyze the transfer characteristics [1, 3]. Topputo [1] and Oshima et al. [3] presented a global map of impulse and time of flight (TOF) for the bi-impulsive transfers within 100 and 200 Days in the Sun-Earth/Moon PBCR4BP, revealing the rich structure of the solution space. Based on their work, Campana and Topputo [28] used the data mining method to extract the transfer families in the Sun-Earth/Moon PBCR4BP. The aforementioned works [1, 3, 28] performed a valuable exploration on the solution space and transfer characteristics of bi-impulsive Earth-Moon transfers in the multi-body problems. However, they did not focus on the distribution of construction parameters. Such analysis can further provide useful insight into selecting high-quality initial guesses and aid in the construction of bi-impulsive transfers. Pinelli [29] pioneered this type of exploration using the neural network method to learn the mapping between construction parameters and generate the initial guesses for trajectory correction accordingly. However, Pinelli [29] mainly focused on one type of transfer trajectory, i.e., exterior transfer without fly-bys. Therefore, a more systematic exploration of the solution space in terms of construction parameters should be performed. Combining with other limitations of the grid search method, we summarize the limitations of the current works on the grid search method to construct Earth-Moon transfers in the multi-body problems:

1. Generally, using the grid search method to generate initial guesses can be considered as a cold-start initialization, which typically yields a relatively low convergence rate.
2. Also, because the grid search method is a cold-start initialization, the corresponding trajectory correction usually requires a long computational time.
3. Current works [1, 3, 28] on the grid search method typically focus on transfer characteristics and transfer families, but pay less attention to the distribution of construction parameters, which can provide further insight into trajectory construction.
4. Current works [1, 3, 28] on the grid search method typically focus on transfers with the specific departure/arrival orbital altitudes (i.e., transfers from a 167 km circular Earth parking orbit to a 100 km circular Moon target orbit). When considering transfers with other altitudes, the process of grid search and trajectory correction should be repeated, with a relatively low convergence rate and computational efficiency.

To address the aforementioned limitations, the main purpose of this paper is to explore a way to augment the traditional grid search method. We firstly focus on the solutions space of bi-impulsive Earth-Moon transfers with different departure/arrival orbital altitudes, in particular, the distribution of construction parameters (departure phase angle at the Earth parking orbit, initial-to-circular velocity ratio, and time of flight (TOF)). An interesting phenomenon about the discontinuous behavior of the TOF distribution for each departure phase angle is discovered. This phenomenon can also be observed for different settings of orbital altitudes. Furthermore, the distributions of TOF and departure phase angle at the Earth parking orbit exhibit similarity, which can provide further insight into constructing transfers with different departure/arrival orbital altitudes. These phenomena about the distribution of construction parameters are new or less-reported compared to current works. Then, a way to utilize these phenomena to aid in trajectory construction and augment the traditional grid search method is explored. An alternative way is to utilize the generative models, such as variational autoencoder (VAE) [30], flow-based model [31] and diffusion model [32]. Compared to the neural network method [29] that depends on the input being close to the distribution of feasible solutions (when the selected inputs lie outside the distribution of feasible solutions, the prediction may provide an inaccurate initial guess and reduce the convergence rate), generative models learn and approximate the distribution of interest. They select samples from a simple distribution (e.g., a standard Gaussian distribution) and then perform a denoising process to generate data samples. These models have been applied to the initial guess generation of multi-body periodic orbits [30], Earth-Mars ballistic transfers [33], and low-thrust transfer trajectories [32]. Among the generative models, the diffusion model has been widely applied due to fewer constraints on model architecture and enhanced ability to capture complex data distributions [32]. Therefore, this paper adopts the diffusion model to aid in generating high-quality initial guesses and augmenting the traditional grid search method. Also, the use of the diffusion model enables the generation of samples with a preset number and is not limited to the original data. This paper combines the dynamical prior knowledge (phenomenon about the distribution of construction parameters) with the diffusion model. Therefore, a diffusion model-augmented grid search method to construct bi-impulsive Earth-Moon transfers with different departure/arrival orbital altitudes is proposed in this paper. The construction results of the proposed method are then presented and discussed. Comparison with the results obtained from the traditional grid search method indicates that the proposed method takes advantage of improved convergence rate and computational efficiency for all three settings of departure/arrival orbital altitudes, while ensuring comparable transfer characteristics.

The rest of this paper is organized as follows. Section 2 presents the bi-impulsive Earth-Moon transfers and the corresponding solution space in the Earth-Moon PCR3BP. Section 3 proposes a diffusion model-augmented grid search method to construct bi-impulsive Earth-Moon transfers with different departure/arrival orbital altitudes. Section 4 presents the construction results and comparison with the traditional grid search method. Finally, conclusions are drawn in Section 5.

2. Three-Body Bi-Impulsive Earth-Moon Transfer

This section introduces the bi-impulsive Earth-Moon transfers in the Earth-Moon PCR3BP, including the dynamical equations of the Earth-Moon PCR3BP, the concept, and solution space of bi-impulsive transfers in the Earth-Moon PCR3BP. The dynamical analysis of the solution space of bi-impulsive Earth-Moon transfers with different departure/arrival orbital altitudes can provide further insight into the training of the diffusion model.

2.1. Earth-Moon PCR3BP

We consider the construction problem of bi-impulsive Earth-Moon transfers in the Earth-Moon PCR3BP. In this model, the Earth, the Moon, and the spacecraft are assumed to move in the same plane, where the Earth and the Moon

move in circular orbit around their barycenter. Selecting the dimensionless units (the length unit (LU) is set as the Earth-Moon distance, the mass unit (MU) is set as the Earth-Moon combined mass, and the time unit (TU) is set as the $1/2\pi$ of the Earth-Moon orbital period around their barycenter) and adopting the Earth-Moon rotating frame, the dynamical equations of the Earth-Moon PCR3BP can be written as:

$$\begin{aligned}
 \dot{x} &= u \\
 \dot{y} &= v \\
 \dot{u} &= x + 2v - \frac{(1-\mu)(x+\mu)}{r_1^3} - \frac{\mu(x+\mu-1)}{r_2^3} \\
 \dot{v} &= y - 2u - \frac{(1-\mu)y}{r_1^3} - \frac{\mu y}{r_2^3} \\
 r_1 &= \sqrt{(x+\mu)^2 + y^2} \quad r_2 = \sqrt{(x+\mu-1)^2 + y^2}
 \end{aligned} \tag{1}$$

where x and y denote the position components with respect to the Earth-Moon barycenter in the Earth-Moon rotating frame, u and v denote the velocity components corresponding to x and y in the Earth-Moon rotating frame, μ denotes the mass parameter of the Earth-Moon PCR3BP which can be expressed as $\mu = m_{\text{Moon}} / (m_{\text{Earth}} + m_{\text{Moon}})$ (m denotes the mass), r_1 denotes the distance between the Earth and the spacecraft, and r_2 denotes the distance between the Moon and the spacecraft. Numerical integration of Eq. (1) achieved by a variable-step, variable-order (VSVO) Adams-Bashforth-Moulton predictor-corrector method (orders 1 to 13) with absolute and relative tolerances set to 1×10^{-13} is performed to obtain trajectories in the Earth-Moon PCR3BP. The parameters used in this paper can be found in Ref. [1]. In this paper, bi-impulsive Earth-Moon transfers are constructed in this model. Subsequently, the concept and solution space of bi-impulsive Earth-Moon transfers in this model are introduced.

2.2. Concept of Bi-impulsive Earth-Moon Transfers

In this paper, we focus on the classical Earth-Moon transfers, particularly the bi-impulsive ones. This type of transfer describes a scenario where the spacecraft is sent to the transfer trajectory from a circular Earth parking orbit with the altitude h_i using an Earth injection impulse Δv_i , and enters a circular Moon target orbit with the altitude h_f using a Moon insertion impulse Δv_f . Tangential impulses are performed, and then the states of the transfer trajectories should satisfy the following constraints [1]:

$$\boldsymbol{\psi}_i = \begin{bmatrix} (x_i + \mu)^2 + y_i^2 - (R_{\text{Earth}} + h_i)^2 \\ (x_i + \mu)(u_i - y_i) + y_i(v_i + x_i + \mu) \end{bmatrix} = \mathbf{0} \tag{2}$$

$$\boldsymbol{\psi}_f = \begin{bmatrix} (x_f + \mu - 1)^2 + y_f^2 - (R_{\text{Moon}} + h_f)^2 \\ (x_f + \mu - 1)(u_f - y_f) + y_f(v_f + x_f + \mu - 1) \end{bmatrix} = \mathbf{0} \tag{3}$$

The subscript “ i ” denotes quantities corresponding to the epoch when the spacecraft departs from the Earth parking orbit, while the subscript “ f ” denotes quantities corresponding to the epoch when the spacecraft enters the Moon target orbit. To construct transfer trajectories satisfying Eqs. (2)-(3), we select the following construction parameters:

$$\mathbf{y} = [\alpha_i, \beta_i, \text{TOF}]^T \tag{4}$$

In these parameters, α_i denotes the departure phase angle of the circular Earth parking orbit in the Earth-Moon rotating frame, β_i denotes the initial-to-circular velocity ratio, and TOF denotes the time of flight. With these parameters, the departure states of transfer trajectories can be expressed following the constraint Eq. (3):

$$\begin{aligned}
 x_i &= r_i \cos \alpha_i - \mu \\
 y_i &= r_i \sin \alpha_i \\
 u_i &= -\left(\beta_i \sqrt{\frac{1-\mu}{r_i}} - r_i \right) \sin \alpha_i \\
 v_i &= \left(\beta_i \sqrt{\frac{1-\mu}{r_i}} - r_i \right) \cos \alpha_i
 \end{aligned} \tag{5}$$

where $r_i = R_{\text{Earth}} + h_i$. Then, the construction of bi-impulsive Earth-Moon transfers is transformed into searching for the feasible solutions integrated from the departure states shown in Eq. (5) within the time interval $[0, \text{TOF}]$ and satisfying the constraint Eq. (3). This paper explores a diffusion model-augmented method to construct the bi-impulsive Earth-Moon transfers in the Earth-Moon PCR3BP. To provide original data and prior knowledge for the training of the diffusion model, the solution space of the bi-impulsive Earth-Moon transfers is firstly presented and analyzed using the grid search method.

2.3. Grid Search Method of Bi-Impulsive Earth-Moon Transfers

In this paper, three groups of h_i and h_f are considered:

$$\begin{aligned}
 \text{Group I: } & h_i = 167 \text{ km}, h_f = 100 \text{ km} \\
 \text{Group II: } & h_i = 167 \text{ km}, h_f = 1500 \text{ km} \\
 \text{Group III: } & h_i = 1500 \text{ km}, h_f = 100 \text{ km}
 \end{aligned} \tag{6}$$

To generate initial guesses, we set \mathbf{y} in Eq. (4) as $\alpha_i \in [0, 2\pi)$ rad with a step-size of $\pi/36$ rad, $\beta_i \in [1.4, 1.414]$ with a step-size of 0.0001, and $\text{TOF} \in [\pi/30, 8\pi]$ TU with a step-size of $\pi/30$ TU. The ranges of α_i and β_i are selected according to Ref. [3], and the selection of TOF does not affect the qualitative findings reported in this paper. With these settings, we obtain 2436480 initial guesses for each group in total. Then, the initial guess is generated from the initial state calculated by Eq. (5).

Once the initial guesses are generated, trajectory correction is performed to make the trajectories satisfy the constraints Eqs. (2)-(3). Trajectory correction can be transformed into a nonlinear programming (NLP) problem. When solving the NLP problem, the sequential quadratic programming (SQP) method is adopted. Since the generated initial guesses satisfy the constraint Eq. (2) rigorously, the constraint of the NLP problem is set as Eq. (3), and the objective function is set to 0. During the trajectory correction, the ranges of the NLP variables are set as $\alpha_i \in (-\infty, \infty)$ rad, $\beta_i \in [1.4, 1.414]$, and $\text{TOF} \in \left[\frac{\pi}{30}, 8\pi \right]$ TU. To ensure the accuracy and efficiency of the SQP method, the parameters used in the trajectory correction are determined through trial and error. The tolerance of the step-size during the iteration is set to 1×10^{-12} , the tolerance of the constraint violation is set to 1×10^{-8} , and the first-order optimality tolerance is set to 1×10^{-6} . Moreover, the maximum number of both iterations and function evaluations are set to 1000. During solving the NLP problem, the Earth/Moon collision trajectories are excluded. When the correction is finished,

the solutions satisfying $\|\psi_f\| < 1 \times 10^{-8}$ are selected and recorded. The values of α_i are then transformed into those within $[0, 2\pi]$ rad.

2.4. Solution Space of Bi-impulsive Earth-Moon Transfers

Using the aforementioned method, we totally obtain 1018001 feasible solutions for Group I, 1132795 solutions for Group II, and 1212226 solutions for Group III. The corresponding solution space is presented in the terms of the (TOF, Δv) map shown in Fig. 1. This type of map has been widely adopted [1, 3] to describe the solution space of the transfers in the multi-body problem. However, although the map provides the full information about the transfer characteristics, it does not provide more information about the distribution of the construction parameters. In this paper, we would like to present the distribution of the construction parameters and report an interesting, novel, or less-reported phenomenon, i.e., the discontinuous behavior of TOF distribution.

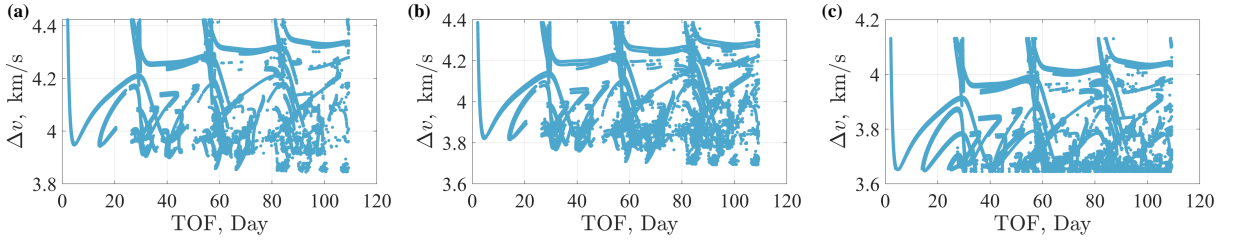


Figure 1: The (TOF, Δv) map of obtained bi-impulsive Earth-Moon transfers in the Earth-Moon PCR3BP. (a) Group I; (b) Group II; (c) Group III.

For the obtained solutions, the (TOF, α_i) map and the (α_i , β_i) map for three groups are presented in Figs. 2-3. The construction parameters for these four groups exhibit similar distributions. Differing from the (α_i , β_i) map, the (TOF, α_i) map reveals a rather pronounced phenomenon:

1. For each α_i , the distribution of TOF reveals a discontinuous behavior. The map can be approximately divided into 5 branches, and the TOF of each branch differs by approximately one month.
2. For each branch, α_i exhibits a banded distribution with respect to TOF, and the slope of α_i with respect to TOF is approximately equal.

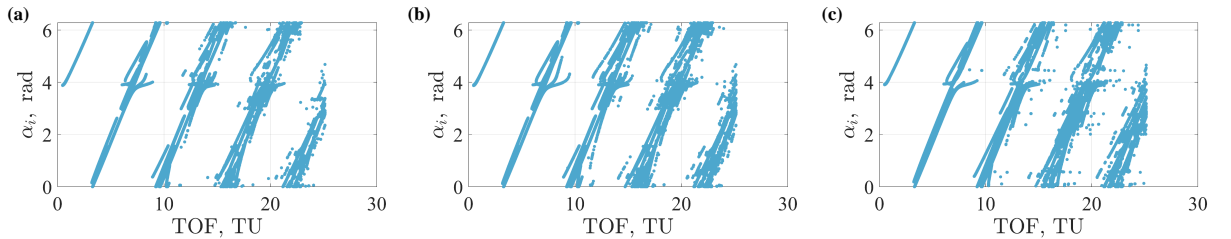


Figure 2: The (TOF, α_i) map of obtained bi-impulsive Earth-Moon transfers in the Earth-Moon PCR3BP. (a) Group I; (b) Group II; (c) Group III.

Diffusion Model-Augmented Construction of Three-Body Earth-Moon Transfers

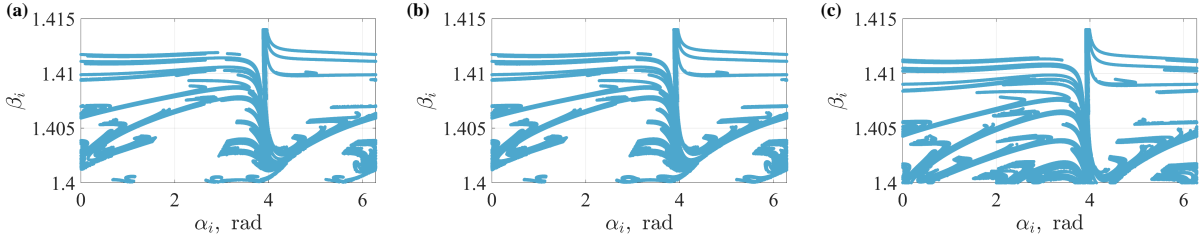


Figure 3: The (α_i, β_i) map of obtained bi-impulsive Earth-Moon transfers in the Earth-Moon PCR3BP. (a) Group I; (b) Group II; (c) Group III.

The aforementioned phenomenon exists in all of three groups, implying its robustness with respect to the orbital altitude settings. Also, when adopting a smaller step-size of construction parameters, a similar phenomenon has been observed for Group I [34], implying its robustness with respect to the grid search settings. This phenomenon is possibly corresponding to the orbital period of the Earth/Moon around their barycenter, and cannot be revealed by the $(\text{TOF}, \Delta v)$ map, as the distribution shown in Fig. 1 reveals a continuity of TOF. It can further provide useful insight into selecting initial guesses to construct transfers, i.e., when performing the grid search, there might be no need to select the values of (TOF, α_i) pair located in the blank region in Fig. 2 (a)-(c). Also, examining the solution space between different groups (see Fig. 4), it can be observed that the (TOF, α_i) maps are similar between solutions with different values of h_i of h_f , while the (α_i, β_i) maps can be different more pronouncedly. This phenomenon motivates us to use the (TOF, α_i) maps to train a diffusion model, as once the model is trained, it can be applied to the construction of bi-impulsive Earth-Moon transfers with different departure/arrival orbital altitudes. Subsequently, a diffusion model-augmented construction method is proposed.

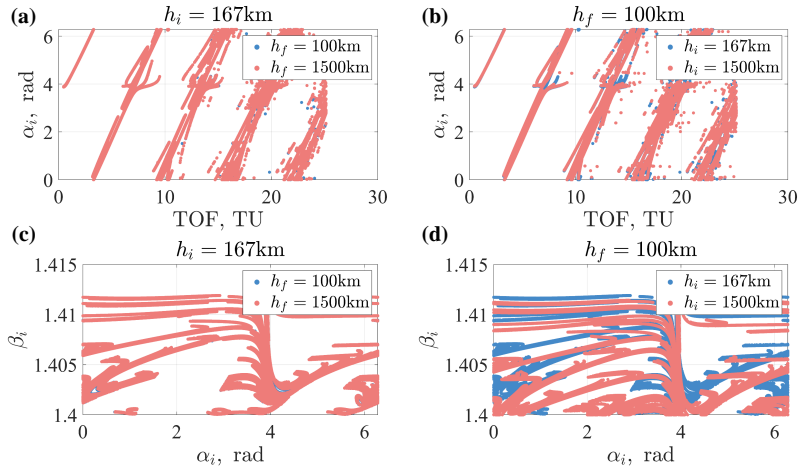


Figure 4: Solution space for different groups. (a) (TOF, α_i) map for Groups I and II; (b) (TOF, α_i) map for Groups I and III; (c) (α_i, β_i) map for Groups I and II; (d) (α_i, β_i) map for Groups I and III.

3. Diffusion Model-Augmented Construction Method of Bi-Impulsive Earth-Moon Transfers

In this section, a diffusion model-augmented method to construct bi-impulsive Earth-Moon transfers mentioned in Section 2 is proposed. Firstly, the dataset for training is prepared based on the aforementioned dynamical analysis. Then,

the training and evaluation of the diffusion model are presented. Finally, a construction method of bi-impulsive Earth-Moon transfers combining the samples generated by the diffusion model with the grid search is proposed, enabling the generation of high-quality initial guesses and improved convergence rate of trajectory correction over the traditional grid search method described in Section 2. The diffusion model is trained in a Python 3.12.12 environment on NVIDIA GeForce RTX 3050 (8 GB VRAM). We set the random seed to 42 to ensure reproducibility.

3.1. Preparation of the Dataset

Based on the dynamical analysis of the solution space mentioned in Section 2, we adopt the (TOF, α_i) map to train the diffusion model. In particular, only the (TOF, α_i) map with $h_i = 167$ km and $h_f = 100$ km (i.e., Group I) is selected due to the similar distributions between different groups shown in Fig. 4 (a) and (b). As shown in Fig. 5, we combine the 5 branches into one branch to simplify the training, using the following mapping:

$$\begin{aligned}
 \alpha_{i\text{Branch } 1} &= \alpha_{i\text{Branch } 1}, \text{TOF}_{\text{Branch } 1} = \text{TOF}_{\text{Branch } 1} \\
 \alpha_{i\text{Branch } 2} &= \alpha_{i\text{Branch } 2} + 2\pi, \text{TOF}_{\text{Branch } 2} = \text{TOF}_{\text{Branch } 2} \\
 \alpha_{i\text{Branch } 3} &= \alpha_{i\text{Branch } 3} + 4\pi, \text{TOF}_{\text{Branch } 3} = \text{TOF}_{\text{Branch } 3} \\
 \alpha_{i\text{Branch } 4} &= \alpha_{i\text{Branch } 4} + 6\pi, \text{TOF}_{\text{Branch } 4} = \text{TOF}_{\text{Branch } 4} \\
 \alpha_{i\text{Branch } 5} &= \alpha_{i\text{Branch } 5} + 8\pi, \text{TOF}_{\text{Branch } 5} = \text{TOF}_{\text{Branch } 5}
 \end{aligned} \tag{7}$$

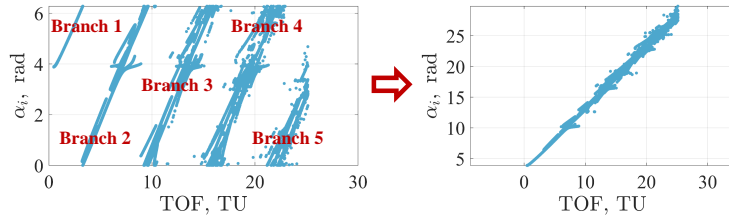


Figure 5: The combined (TOF, α_i) map for Group I.

Once the dataset (i.e., the transformed (TOF, α_i) map shown in Fig. 5) is obtained, we use the *ShuffleSpilt* function from sklearn to divide the dataset into the training dataset (80%) and the validation dataset (20%). Then, we denote the transformed (TOF, α_i) points as \mathbf{x}_0 , and perform a normalization of these data:

$$\tilde{\mathbf{x}}_0 = (\mathbf{x}_0 - \boldsymbol{\mu}_{\text{Training}}) \oslash (\boldsymbol{\sigma}_{\text{Training}} + 1 \times 10^{-6}) \tag{8}$$

where $\boldsymbol{\mu}_{\text{Training}}$ and $\boldsymbol{\sigma}_{\text{Training}}$ denote the mean and standard deviation of the training dataset, and the subscript ‘‘Training’’ denotes quantities corresponding to the training dataset. When generating samples, the inverse normalization is performed. Subsequently, the training of the diffusion model is presented.

3.2. Diffusion Model

When using the diffusion model to generate samples, the samples from a standard Gaussian distribution are firstly selected. Subsequently, these samples are mapped into samples corresponding to a distribution of interest, i.e., the expected samples [32] (generated (TOF, α_i) samples in this paper). This process is denoted as the reverse denoising process. Moreover, to train a diffusion model, the forward diffusion process is required. Therefore, the diffusion model

can typically be divided into two processes, i.e., the forward diffusion process and reverse denoising process (shown in Fig. 6). Then, the details about these processes are introduced, and the training of the diffusion model is presented.

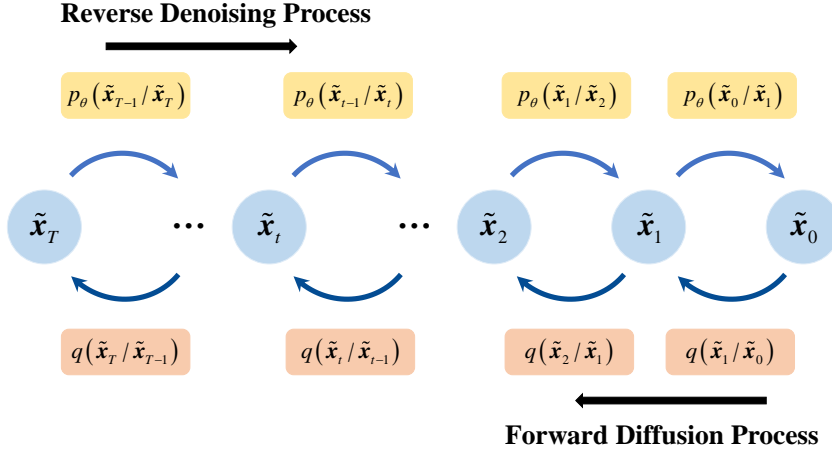


Figure 6: Schematic of the forward diffusion process and reverse denoising process.

3.2.1. Forward Diffusion Process and Reverse Denoising Process

The forward diffusion process describes a scenario where the Gaussian noise is gradually added into the samples $\tilde{\mathbf{x}}_0$, and finally makes the samples approximated as an approximately standard Gaussian noise, i.e., $p(\tilde{\mathbf{x}}_T) \approx \mathcal{N}(\tilde{\mathbf{x}}_T; \mathbf{0}, \mathbf{I})$, where T denotes the total diffusion step and \mathbf{I} is the identity matrix. To achieve this target, $q(\tilde{\mathbf{x}}_t|\tilde{\mathbf{x}}_{t-1})$ in the forward diffusion process is presented as (in Fig. 6, t denotes an intermediate diffusion step):

$$q(\tilde{\mathbf{x}}_t|\tilde{\mathbf{x}}_{t-1}) = \mathcal{N}(\tilde{\mathbf{x}}_t; \sqrt{a_t}\tilde{\mathbf{x}}_{t-1}, b_t\mathbf{I}), \quad a_t = 1 - b_t \quad (9)$$

where b_t denotes the noise variance at diffusion step t , and $\{b_t\}_{t=1}^T$ denotes the variance schedule. In this paper, the linear variance schedule is adopted [35]:

$$b_t = b_{\min} + \frac{t-1}{T-1} (b_{\max} - b_{\min}) \quad (10)$$

where $b_{\min} = 1 \times 10^{-4}$, $b_{\max} = 0.02$, and $T = 1000$. With Eq. (9), $\tilde{\mathbf{x}}_t$ can be constructed explicitly from $\tilde{\mathbf{x}}_0$:

$$\tilde{\mathbf{x}}_t = \sqrt{\bar{a}_t}\tilde{\mathbf{x}}_0 + \sqrt{1-\bar{a}_t}\epsilon, \quad \epsilon \sim \mathcal{N}(\epsilon; \mathbf{0}, \mathbf{I}) \quad (11)$$

where:

$$\bar{a}_t = \prod_{s=1}^t a_s \quad (12)$$

In the reverse denoising process, samples from the standard Gaussian distribution are selected, and the noise $\epsilon_\theta(\tilde{\mathbf{x}}_t, t)$ is removed iteratively. During this process, a neural network with parameters θ is used to predict the noise $\epsilon_\theta(\tilde{\mathbf{x}}_t, t)$.

In Fig. 6, $p_\theta(\tilde{\mathbf{x}}_{t-1}|\tilde{\mathbf{x}}_t)$ is written as:

$$p_\theta(\tilde{\mathbf{x}}_{t-1}|\tilde{\mathbf{x}}_t) = \mathcal{N}\left(\tilde{\mathbf{x}}_{t-1}; \boldsymbol{\mu}_\theta(\tilde{\mathbf{x}}_t, t), \widehat{b}_t \mathbf{I}\right), \widehat{b}_t = b_t \frac{1 - \bar{a}_{t-1}}{1 - \bar{a}_t} \quad (13)$$

where:

$$\boldsymbol{\mu}_\theta(\tilde{\mathbf{x}}_t, t) = \frac{1}{\sqrt{a_t}} \left(\tilde{\mathbf{x}}_t - \frac{b_t}{\sqrt{1 - \bar{a}_t}} \boldsymbol{\epsilon}_\theta(\tilde{\mathbf{x}}_t, t) \right) \quad (14)$$

Therefore, the predicted $\tilde{\mathbf{x}}_{t-1}$ can be obtained as:

$$\tilde{\mathbf{x}}_{t-1} = \begin{cases} \boldsymbol{\mu}_\theta(\tilde{\mathbf{x}}_t, t) + \sqrt{\widehat{b}_t} \mathbf{z}, \mathbf{z} \sim \mathcal{N}(\mathbf{z}; \mathbf{0}, \mathbf{I}), t > 1 \\ \boldsymbol{\mu}_\theta(\tilde{\mathbf{x}}_t, t), t = 1 \end{cases} \quad (15)$$

Based on the aforementioned framework, samples corresponding to a distribution of interest can be generated, which can consequently provide high-quality initial guesses for bi-impulsive Earth-Moon transfer construction. Subsequently, the training and evaluation of the diffusion model in this paper are presented.

3.2.2. Training and Evaluation of the Diffusion Model

Using the training dataset and validation dataset mentioned in Section 3.1, the training and evaluation of the diffusion model are presented. In this paper, a time-conditioned residual multilayer perceptron (MLP) is adopted as the neural network to predict the noise, whose structure is shown in Fig. 7. The input of the neural network is set as $\tilde{\mathbf{x}}_{t_{\text{Training}}}$ and diffusion step t_{Training} . In particular, the diffusion step t is transformed into a 64-dimensional time embedding using a sinusoidal embedding [36] followed by a time embedding (64 \rightarrow 256 \rightarrow 64) MLP. The resulting time embedding is further projected in each residual block to generate FiLM scale and shift parameters, as shown in Fig. 7. The sinusoidal embedding can be written as:

$$\begin{aligned} \boldsymbol{\gamma}(t_{\text{Training}}) &\in \mathbb{R}^{64} \\ \boldsymbol{\gamma}(t_{\text{Training}}) &= [\sin(t_{\text{Training}}\omega_0), \dots, \sin(t_{\text{Training}}\omega_{31}), \cos(t_{\text{Training}}\omega_0), \dots, \cos(t_{\text{Training}}\omega_{31})] \\ \omega_i &= \frac{1}{10000 \frac{i}{64/2-1}}, i = 0, 1, \dots, 31 \end{aligned} \quad (16)$$

The output of the neural network is set as $\boldsymbol{\epsilon}_\theta(\tilde{\mathbf{x}}_{t_{\text{Training}}}, t_{\text{Training}})$. In Fig. 7, the term ‘‘LN’’ denotes layer normalization. When training the neural network to predict the noise, the batch size is fixed as 1024. For each mini-batch, $\tilde{\mathbf{x}}_{0_{\text{Training}}}$ are selected from the training dataset using a shuffled *DataLoader*. For each $\tilde{\mathbf{x}}_{0_{\text{Training}}}$, t_{Training} and $\boldsymbol{\epsilon}_{\text{Training}}$ are sampled:

$$\begin{aligned} t_{\text{Training}} &\sim \mathcal{U}\{1, \dots, T\} \\ \boldsymbol{\epsilon}_{\text{Training}} &\sim \mathcal{N}(\boldsymbol{\epsilon}_{\text{Training}}; \mathbf{0}, \mathbf{I}) \end{aligned} \quad (17)$$

Then, $\tilde{\mathbf{x}}_{t_{\text{Training}}}$ can be obtained by Eq. (11). Then, the neural network predicts the predicted noise $\epsilon_{\theta}(\tilde{\mathbf{x}}_{t_{\text{Training}}}, t_{\text{Training}})$. We adopt the mean squared error (MSE) between $\epsilon_{\text{Training}}$ and $\epsilon_{\theta}(\tilde{\mathbf{x}}_{t_{\text{Training}}}, t_{\text{Training}})$ as the loss function [35]:

$$\text{Loss}_{\text{Training}}(\theta) = \mathbb{E}_{\tilde{\mathbf{x}}_{0\text{Training}}, t_{\text{Training}}, \epsilon_{\text{Training}}} \left[\left\| \epsilon_{\text{Training}} - \epsilon_{\theta}(\tilde{\mathbf{x}}_{t_{\text{Training}}}, t_{\text{Training}}) \right\|^2 \right] \quad (18)$$

Based on the aforementioned discussion, the training framework of the used neural network can be summarized as follows:

1. *Structure of the neural network:* A time-conditioned residual MLP is adopted as the neural network to predict the noise, and the schematic of its structure is shown in Fig. 7. For this structure, the number of time-conditioned residual blocks (L) and hidden dimension (H) are treated as the hyperparameters (see Table 1).
2. *Training process:* The *Adam* optimizer is employed, and gradients are clipped with a maximum norm of 1.0. The loss function is set as Eq. (18), and the learning rate (lr) is treated as the hyperparameter (see Table 1). The batch size is fixed as 1024. For each mini-batch iteration, a mini-batch estimate of the loss function shown in Eq. (18) is calculated and the parameters θ of the neural network are updated. The training epoch is set to 500. When recording the loss function corresponding to the training dataset for each epoch, the weighted average with respect to each mini-batch is adopted.

Table 1: Settings of Hyperparameters

Hyperparameter	Setting
L	4, 8, 16
H	64, 128, 256
lr	1×10^{-3} , 1×10^{-4} , 1×10^{-5}

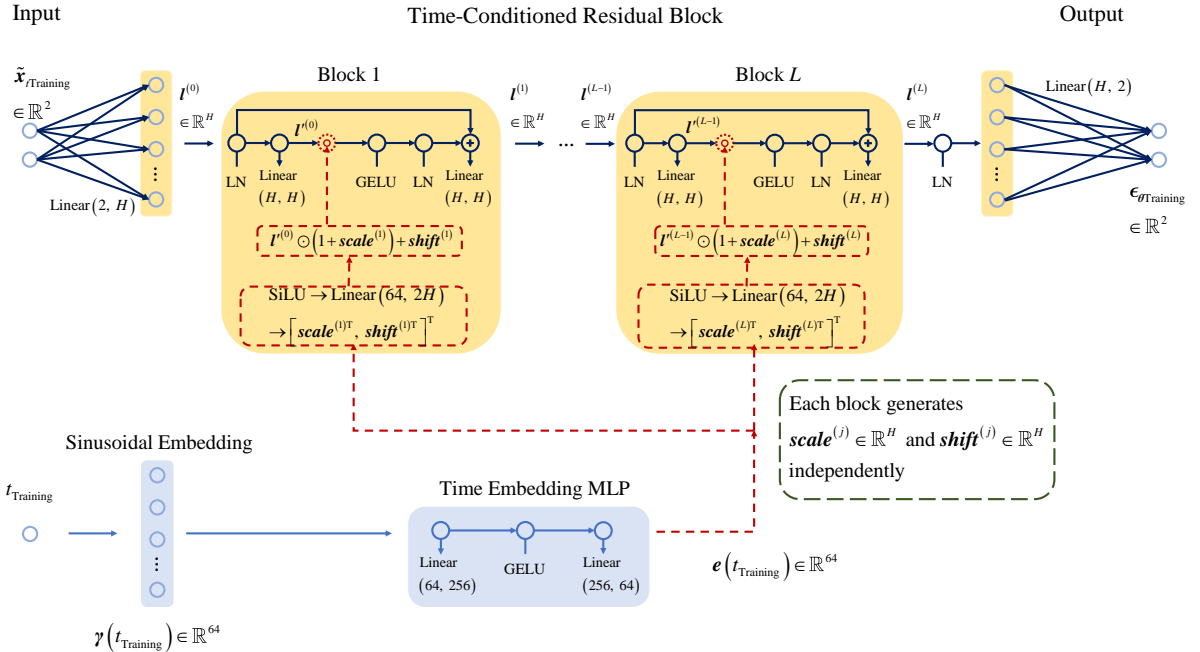


Figure 7: Schematic of the structure of the neural network.

When evaluating the performance of the neural network and selecting the optimal hyperparameter combination, the validation dataset is employed. For each validation mini-batch, $\tilde{\mathbf{x}}_{0\text{Validation}}$ are selected using a *DataLoader* which is not shuffled. The Monte Carlo validation is performed, and $t_{\text{Validation}}$ and $\epsilon_{\text{Validation}}$ are sampled 8 times (i.e., $t_{\text{Validation}}^{(k)}$ and $\epsilon_{\text{Validation}}^{(k)}$, $k = 1, \dots, 8$) to calculate the loss function corresponding to the validation dataset:

$$\text{Loss}_{\text{Validation}}(\theta) = \frac{1}{8} \sum_{k=1}^8 \mathbb{E}_{\tilde{\mathbf{x}}_{0\text{Validation}}, t_{\text{Validation}}^{(k)}, \epsilon_{\text{Validation}}^{(k)}} \left[\left\| \epsilon_{\text{Validation}}^{(k)} - \epsilon_{\theta} \left(\tilde{\mathbf{x}}_{t_{\text{Validation}}^{(k)}}, t_{\text{Validation}}^{(k)} \right) \right\|^2 \right] \quad (19)$$

During the training, we record the minimum $\text{Loss}_{\text{Validation}}(\theta)$ and the corresponding epoch for each hyperparameter combination. We select the optimal hyperparameter combination with the minimum $\text{Loss}_{\text{Validation}}(\theta)$ among these 27 combinations and the corresponding best epoch (E_{best}). Then, we combine the training dataset and validation dataset, and perform a retraining. The epoch of retraining is set as $\max \left(1, \left\lfloor E_{\text{best}} \frac{N_{\text{Training}} + N_{\text{Validation}}}{N_{\text{Training}}} \right\rfloor \right)$ (where N denotes the sample number). Once the retraining is completed, the (TOF, α_i) samples can be generated.

3.2.3. Generation of New Samples

When using the trained diffusion model to generate new samples, we select 20736 points from a standard Gaussian distribution:

$$\tilde{\mathbf{x}}_{T\text{Generated}} \sim \mathcal{N}(\tilde{\mathbf{x}}_{T\text{Generated}}; \mathbf{0}, \mathbf{I}) \quad (20)$$

Then, we use the trained neural network to predict the noise and perform a reverse denoising process shown in Eq. (15) to obtain $\tilde{\mathbf{x}}_{0\text{Generated}}$. Finally, the inverse normalization is performed:

$$\mathbf{x}_{0\text{Generated}} = \tilde{\mathbf{x}}_{0\text{Generated}} \odot \sigma_{\text{Training}} + \mu_{\text{Training}} \quad (21)$$

Subsequently, with $\mathbf{x}_{0\text{Generated}}$, we propose a diffusion model-augmented grid search method to construct bi-impulsive Earth-Moon transfers with different departure/arrival orbital altitudes.

3.3. Diffusion Model-Augmented Grid Search Method

To improve the convergence rate and computational efficiency of the traditional grid search method, we use the aforementioned diffusion model to augment this type of method. The main steps of the proposed diffusion model-augmented grid search method are summarized as follows:

1. Transforming α_i in $\mathbf{x}_{0\text{Generated}}$ into $[0, 2\pi]$ rad, and selecting $\text{TOF} \in \left[\frac{\pi}{30}, 8\pi \right]$ TU in $\mathbf{x}_{0\text{Generated}}$ and the corresponding α_i .
2. Combining the transformed/selected (TOF, α_i) from $\mathbf{x}_{0\text{Generated}}$ with $\beta_i \in [1.4, 1.414]$ with a step-size of 0.0001 to generate initial guesses. All three groups of altitude settings shown in Eq. (6) are considered.
3. Performing the trajectory correction following the settings mentioned in Section 2.3.

Subsequently, the construction results of the proposed method are presented and discussed in Section 4. The advantages over the traditional grid search method are also revealed according to the comparison between these two methods.

4. Results and Discussion

This section presents the results of this paper. Firstly, the loss time history for the aforementioned hyperparameter combinations is presented, which determines the optimal hyperparameter combination with the minimum validation loss. Then, the new samples are generated from the retrained diffusion model, and the diffusion model-augmented grid search method is performed to construct the solution space of bi-impulsive Earth-Moon transfers with different departure/arrival orbital altitudes. Finally, the comparison between the diffusion model-augmented grid search method and the traditional grid search method is performed to reveal the advantages of the proposed method. We perform the trajectory correction on two shared-memory multi-core CPUs (96 cores), and use a loop-level parallelism in the outer loop. Two Intel Xeon Platinum 8488C processors (2.4 GHz base frequency and 256 GB RAM) in a Linux environment are used in the simulations.

4.1. Selection of the Optimal Hyperparameter Combination

The loss time history for the aforementioned hyperparameter combinations is presented in Fig. 8, where the solid curves denote the training loss while the dashed curves denote the validation loss. From Fig. 8, it can be observed that the model does not exhibit obvious overfitting during training. Then, we select the optimal hyperparameter combination with the minimum validation loss and the best epoch.

Diffusion Model-Augmented Construction of Three-Body Earth-Moon Transfers

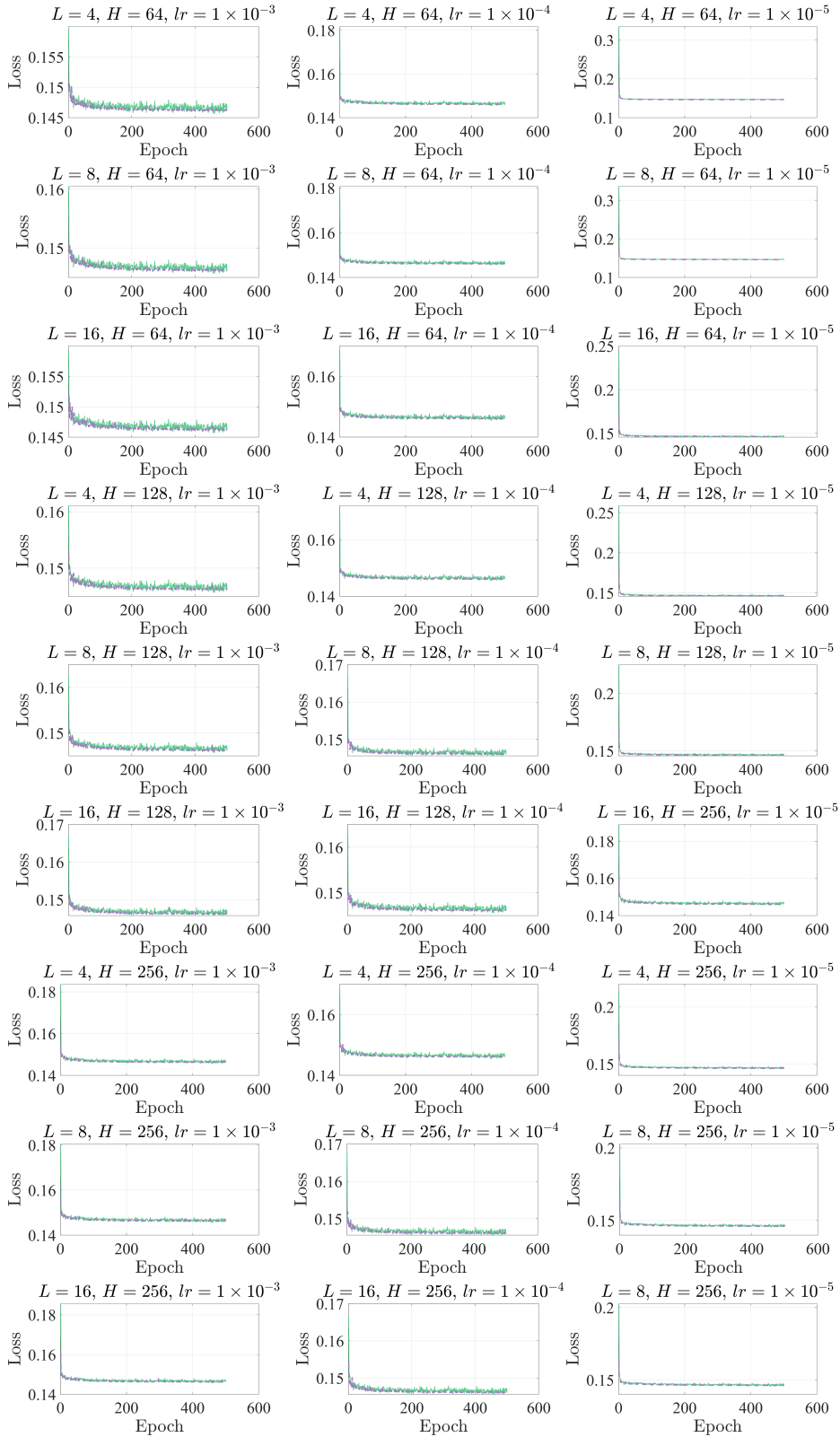


Figure 8: The loss time history for the aforementioned hyperparameter combinations.

Table 2: Minimum Validation Loss and the Corresponding Best Epoch for the Aforementioned Hyperparameter Combinations

L	H	lr	$\text{Loss}_{\text{Validation}}$	E_{best}
4	64	1×10^{-3}	0.146100	389
4	64	1×10^{-4}	0.146007	475
4	64	1×10^{-5}	0.146426	481
8	64	1×10^{-3}	0.146057	449
8	64	1×10^{-4}	0.146006	482
8	64	1×10^{-5}	0.146191	496
16	64	1×10^{-3}	0.146089	424
16	64	1×10^{-4}	0.146005	482
16	64	1×10^{-5}	0.146090	499
4	128	1×10^{-3}	0.146103	389
4	128	1×10^{-4}	0.145998	424
4	128	1×10^{-5}	0.146254	481
8	128	1×10^{-3}	0.146093	496
8	128	1×10^{-4}	0.146013	475
8	128	1×10^{-5}	0.146124	499
16	128	1×10^{-3}	0.146099	396
8	128	1×10^{-4}	0.146021	482
8	128	1×10^{-5}	0.146016	500
4	256	1×10^{-3}	0.146127	485
4	256	1×10^{-4}	0.145993	475
4	256	1×10^{-5}	0.146125	500
8	256	1×10^{-3}	0.146105	389
8	256	1×10^{-4}	0.146007	422
8	256	1×10^{-5}	0.146001	482
16	256	1×10^{-3}	0.146098	389
16	256	1×10^{-4}	0.146011	470
16	256	1×10^{-5}	0.146009	475

Table 2 presents the minimum validation loss and the corresponding best epoch for each hyperparameter combination. We select the optimal hyperparameter combination with the minimum validation loss in Table 2:

$$L = 4, H = 256, lr = 1 \times 10^{-4} \quad (22)$$

Then, with this optimal hyperparameter combination, we combine the training dataset and validation dataset, and retrain the diffusion model following the method mentioned in Section 3.2.2. The loss time history of retraining is presented in Fig. 9.

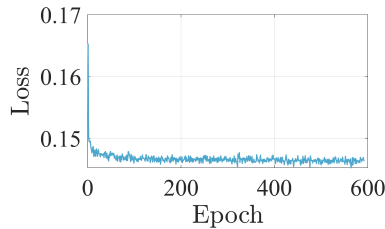


Figure 9: The loss time history of retraining.

Once the retraining is completed, the new samples are generated, as shown in Fig. 10.

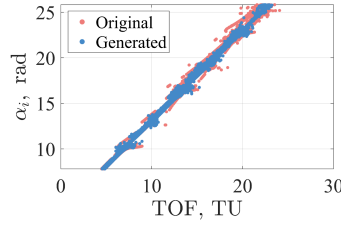


Figure 10: The generated samples.

Then, with the generated samples, the proposed diffusion model-augmented grid search method is applied to the construction of bi-impulsive Earth-Moon transfers. Notably, the application of the generated samples is not only limited to constructing Earth-Moon transfers with $h_i = 167$ km and $h_f = 100$ km, but also with Groups II and III because of the similar (TOF, α_i) distributions shown in Fig. 4 (a) and (b). Subsequently, the construction results are presented and discussed.

4.2. Construction Results of Diffusion Model-Augmented Grid Search Method

Following Step 1 in Section 3.3, we obtain 2920815 initial guesses for Groups I-III, respectively. Figure 11 presents the $(\text{TOF}, \Delta v)$ map of bi-impulsive Earth-Moon transfers in the Earth-Moon PCR3BP obtained from the diffusion model-augmented grid search method. Using the diffusion model-augmented grid search method, we totally obtain 1906844 feasible solutions for Group I, 2040593 solutions for Group II, and 2141073 solutions for Group III. These results preliminarily verify the effectiveness of the proposed diffusion model-augmented grid search method.

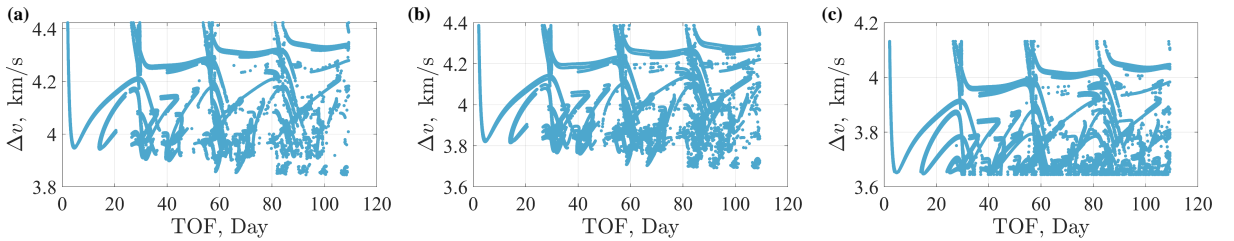


Figure 11: The $(\text{TOF}, \Delta v)$ map of bi-impulsive Earth-Moon transfers in the Earth-Moon PCR3BP obtained from the diffusion model-augmented grid search method. (a) Group I; (b) Group II; (c) Group III.

We extract the Pareto front of the $(\text{TOF}, \Delta v)$ map shown in Fig. 11, considering a shorter TOF and lower Δv , and select typical trajectory samples on the Pareto front. The Pareto fronts for Groups I-III are presented in Figs. 12-14. The red stars denote the corresponding $(\text{TOF}, \Delta v)$ of the selected trajectory samples. Figures 15-17 present the typical trajectory samples selected on the Pareto fronts.

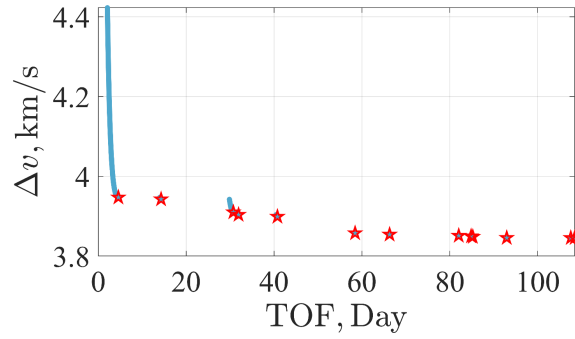


Figure 12: Pareto front of the (TOF, Δv) map (Group I).

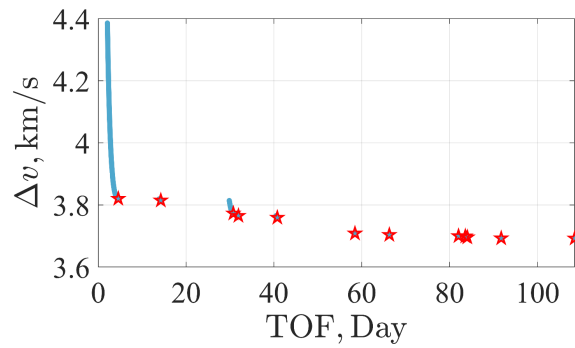


Figure 13: Pareto front of the (TOF, Δv) map (Group II).

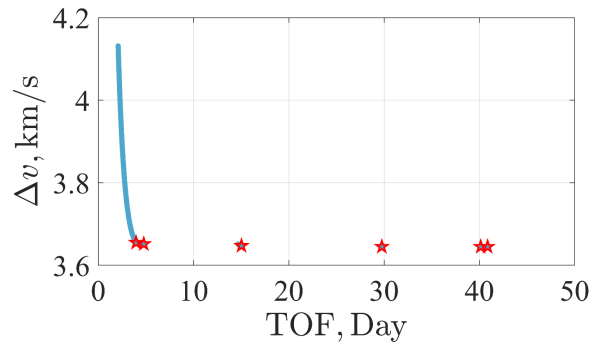


Figure 14: Pareto front of the (TOF, Δv) map (Group III).

Diffusion Model-Augmented Construction of Three-Body Earth-Moon Transfers

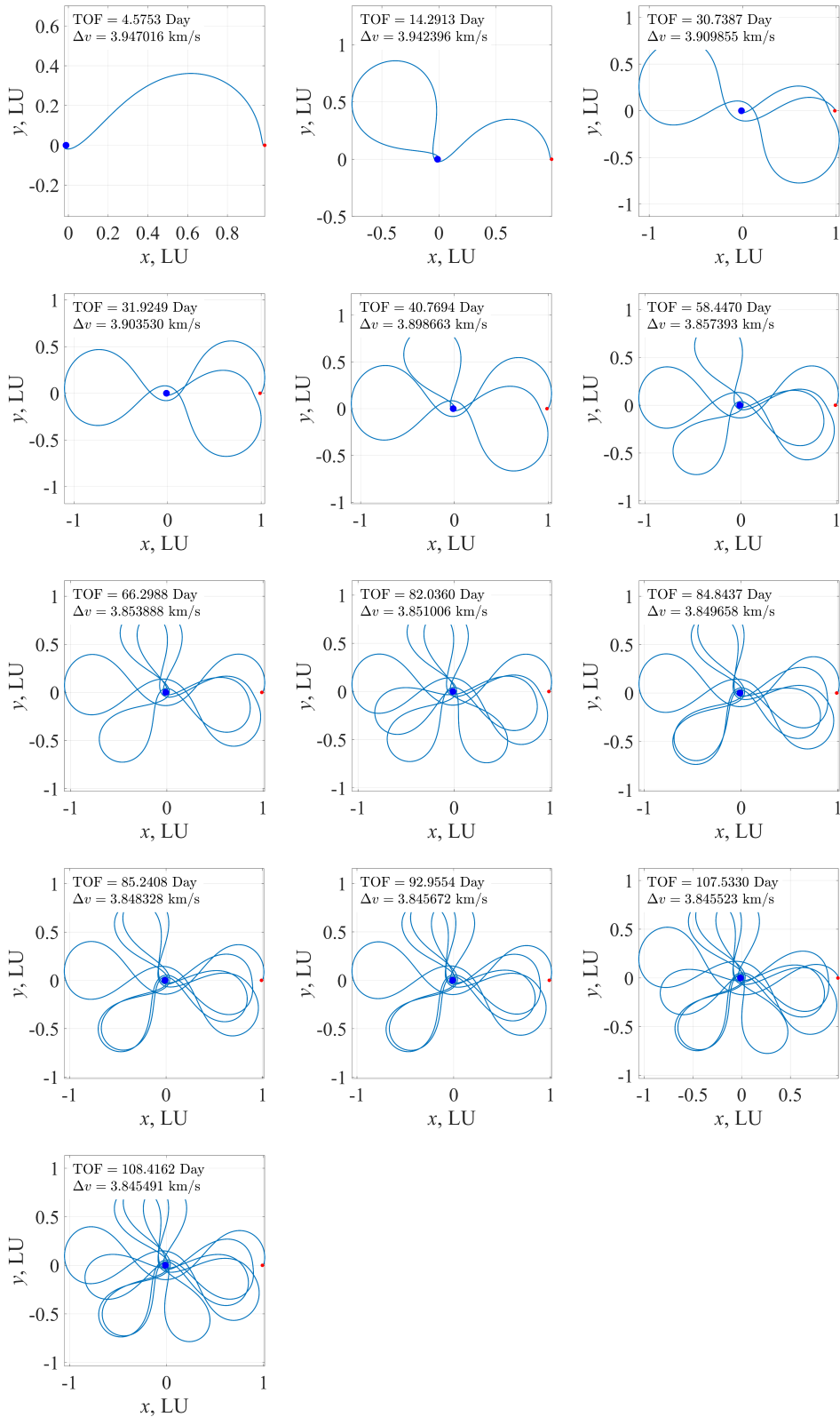


Figure 15: Selected trajectory sample (Group I).

Diffusion Model-Augmented Construction of Three-Body Earth-Moon Transfers

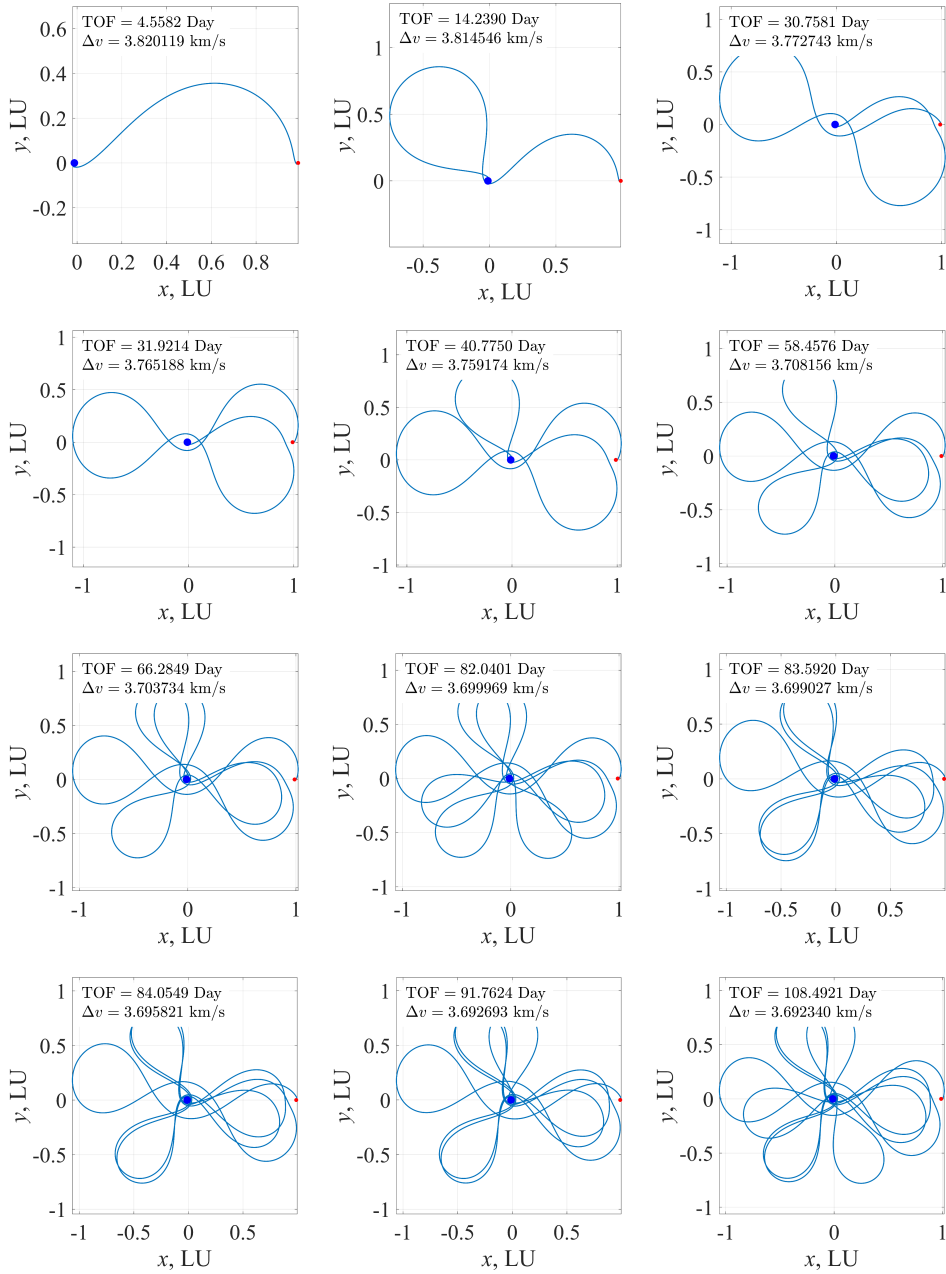


Figure 16: Selected trajectory sample (Group II).

Diffusion Model-Augmented Construction of Three-Body Earth-Moon Transfers

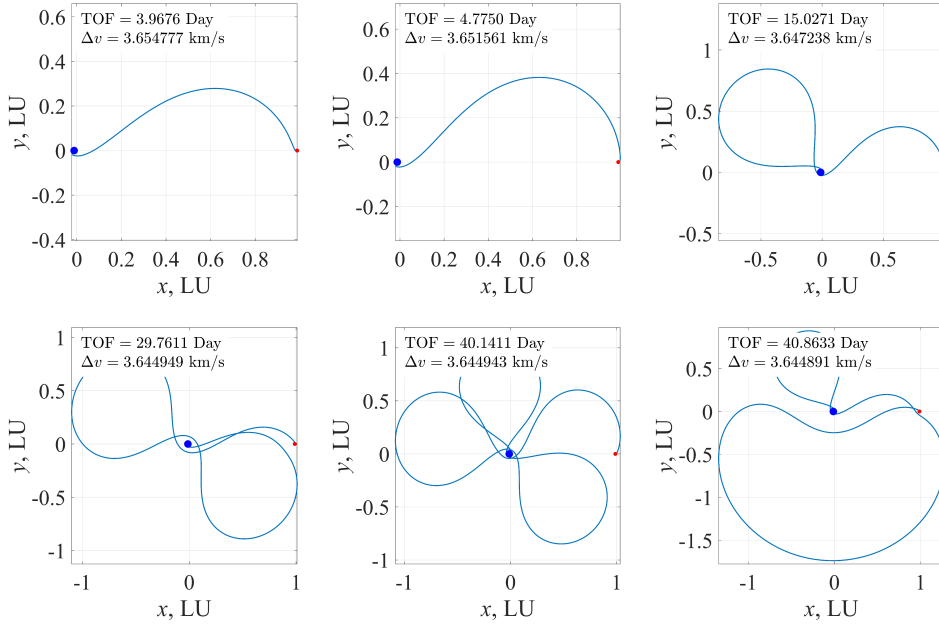


Figure 17: Selected trajectory sample (Group III).

Subsequently, the comparison between results obtained from the proposed diffusion model-augmented grid search method and the traditional grid search method (mentioned in Section 2.3) is performed to reveal the advantages of the developed method.

4.3. Comparison with the Traditional Grid Search Method

The comparison with the traditional grid search method can be divided into three aspects: transfer characteristics, convergence rate, and computational efficiency. Firstly, a comparison in terms of transfer characteristics is performed. Figure 18 presents the extracted Pareto fronts obtained from these two methods. From Fig. 18, it can be observed that the Pareto fronts exhibit similarity between the two methods, indicating the similar transfer characteristics of the solution space obtained from the two methods. These comparison results imply that the use of the diffusion model does not significantly affect the completeness of the solution space. This statement can be further supported by the comparison result in terms of the obtained minimum Δv solution shown in Table 3, as the minimum Δv solutions obtained from the proposed method are comparable to those obtained from the grid search method, for all three groups. These comparison results indicate that the proposed diffusion model-augmented method can generate a solution space with comparable transfer characteristics compared to the traditional grid search method. Then, on the basis of the comparable transfer characteristics, we further compare the two methods in terms of convergence rate and computational efficiency.

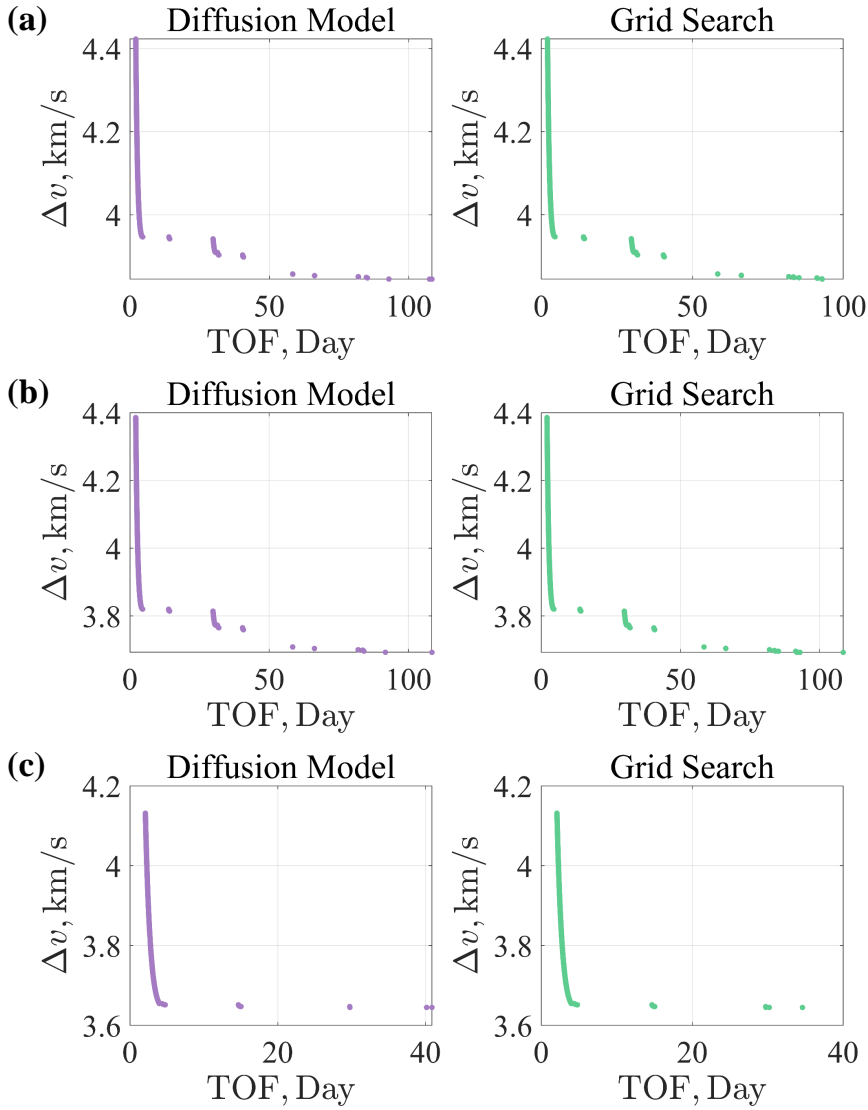


Figure 18: Pareto fronts obtained from the two methods. (a) Group I; (b) Group II; (c) Group III.

Table 3: Comparison Result in terms of the Obtained Minimum Δv Solution

Group	Grid Search, km/s	Proposed, km/s
I	3.845075	3.845491
II	3.692284	3.692340
III	3.644816	3.644891

Table 4 presents the convergence rate obtained from these two methods. It can be found that the use of the diffusion model-augmented method can further improve the convergence rate of the trajectory correction, indicating the high-quality initial guesses generated by the diffusion model. From Table 4, the relative improvement of the convergence rate over the traditional grid search method is 47.34-56.25% relatively, which can be considered as a remarkable advantage of the proposed method. Also, Table 4 presents the wall-clock time of trajectory correction obtained from these two methods. It can be observed that the proposed method saves the wall-clock time more than 39.39% over the traditional

method. These comparison results show that the proposed method takes advantage over the traditional grid search method in the convergence rate and computational efficiency using the high-quality initial guesses obtained from the diffusion model, further strengthening the motivation to combine the generative model with trajectory construction. Notably, the aforementioned phenomenon and construction results are presented in the Earth-Moon PCR3BP. When considering the Sun-Earth/Moon PBCR4BP or other higher-fidelity models, the distribution of (TOF, α_i) and transfer solution space might be more complex due to the additional construction parameters [29]. How to explore and utilize the solution space of the bi-impulsive Earth-Moon transfers in these models remains an open problem.

Table 4: Comparison Result in terms of Convergence Rate

Group	Grid Search	Proposed
I	1018001/2436480 (41.78%)	1906844/2920815 (65.28%)
II	1132795/2436480 (46.49%)	2040593/2920815 (69.86%)
III	1212226/2436480 (49.75%)	2141073/2920815 (73.30%)

Table 5: Comparison Result in terms of Wall-Clock Time of Trajectory Correction

Group	Grid Search, s	Proposed, s
I	2.6449×10^5	1.6032×10^5
II	2.2349×10^5	1.6083×10^5
III	1.9142×10^5	1.1386×10^5

5. Conclusion

Construction of bi-impulsive Earth-Moon transfers with different departure/arrival orbital altitudes in the Earth-Moon planar circular restricted three-body problem is investigated in this paper. Firstly, the solution space of bi-impulsive transfers with different departure/arrival orbital altitudes is analyzed, in particular in terms of construction parameters, including departure phase angle at the Earth parking orbit, initial-to-circular velocity ratio, and time of flight. An interesting phenomenon about the time-of-flight distribution with respect to departure phase angle is discovered. Meanwhile, this type of distribution is similar between different departure/arrival orbital altitudes, which provides insight into the selection of the dataset to train a diffusion model. Then, a diffusion model is trained based on these phenomena, and a diffusion model-augmented grid search method is proposed to improve the convergence rate and computational efficiency of the traditional grid search method. For the construction of transfers with three settings of orbital altitudes, the proposed method improves the convergence rate by 47.34-56.25% and saves the wall-clock time by 39.39-40.52% over the traditional grid search method relatively, while ensuring comparable transfer characteristics. This paper combines the training of a diffusion model with the multi-body dynamical phenomenon, augmenting the traditional grid search method and enabling convenient construction of Earth-Moon transfers with different departure/arrival orbital altitudes.

Declaration of competing interest

The authors declare that they have no known competing financial interests or personal relationships that could have appeared to influence the work reported in this paper.

Acknowledgements

This work was supported by the National Natural Science Foundation of China (Grant Nos. 12525204, 12372044, and U23B6002).

References

- [1] F. Topputo, On optimal two-impulse earth–moon transfers in a four-body model, *Celest. Mech. Dyn. Astron.* 117 (2013) 279–313. doi:10.1007/s10569-013-9513-8.
- [2] Y. Qi, S. Xu, Optimal earth-moon transfers using lunar gravity assist in the restricted four-body problem, *Acta Astronaut.* 134 (2017) 106–120. doi:10.1016/j.actaastro.2017.02.002.
- [3] K. Oshima, F. Topputo, T. Yanao, Low-energy transfers to the moon with long transfer time, *Celest. Mech. Dyn. Astron.* 131 (2019) 1–19. doi:10.1007/s10569-019-9883-7.
- [4] J. Demeyer, P. Gurfil, Transfer to distant retrograde orbits using manifold theory, *J. Guid. Control Dyn.* 30 (5) (2007) 1261–1267. doi:10.2514/1.24960.
- [5] Y. Yin, M. Wang, Y. Shi, H. Zhang, Midcourse correction of earth-moon distant retrograde orbit transfer trajectories based on high-order state transition tensors, *Astrodynamics* 7 (3) (2023) 335–349. doi:10.1007/s42064-023-0162-8.
- [6] M. Wang, C. Zhang, H. Zhang, Mechanism analysis of the dro low-energy transfer problem: An energy perspective, *Astrodynamics* 9 (2) (2025) 165–193. doi:10.1007/s42064-024-0215-7.
- [7] G. Mingotti, P. Gurfil, Mixed low-thrust invariant-manifold transfers to distant prograde orbits around mars, *J. Guid. Control Dyn.* 33 (6) (2010) 1753–1764. doi:10.2514/1.49810.
- [8] G. Mingotti, F. Topputo, F. Bernelli-Zazzera, Transfers to distant periodic orbits around the moon via their invariant manifolds, *Acta Astronaut.* 79 (2012) 20–32. doi:10.1016/j.actaastro.2012.04.022.
- [9] J. S. Parker, R. L. Anderson, *Low-energy lunar trajectory design*, Vol. 12, John Wiley & Sons, 2014.
- [10] C. Du, O. L. Starinova, Y. Liu, Transfer between the planar lyapunov orbits around the earth-moon l2 point using low-thrust engine, *Acta Astronaut.* 201 (2022) 513–525. doi:10.1016/j.actaastro.2022.09.056.
- [11] K. Oshima, A graph-based framework of low-energy transfer design, *Acta Astronaut.* 229 (2025) 644–661. doi:10.1016/j.actaastro.2025.01.050.
- [12] Z. Zhang, X. Hou, Transfer orbits to the earth–moon triangular libration points, *Adv. Space Res.* 55 (12) (2015) 2899–2913. doi:10.1016/j.asr.2015.03.008.
- [13] L. R. Capdevila, K. C. Howell, A transfer network linking earth, moon, and the triangular libration point regions in the earth-moon system, *Adv. Space Res.* 62 (7) (2018) 1826–1852. doi:10.1016/j.asr.2018.06.045.
- [14] Y. Yin, Y. Shi, H. Zhang, A graph-based framework for robust low-energy transfer design in multi-body system, *Acta Astronaut.* 248 (2026) 449–467. doi:10.1016/j.actaastro.2026.06.018.
- [15] R. H. Battin, *An introduction to the mathematics and methods of astrodynamics*, AIAA, 1999.
- [16] H. Pernicka, D. Scarberry, S. Marsh, T. Sweetser, A search for low delta-v earth-to-moon trajectories, in: *Astrodynamics Conference*, AIAA-94-3772-CP, AIAA, Scottsdale, 1994, pp. 530–537. doi:10.2514/6.1994-3772.
- [17] Q. Guo, H. Lei, Families of earth–moon trajectories with applications to transfers towards sun–earth libration point orbits, *Astrophys. Space Sci.* 364 (3) (2019) 43. doi:10.1007/s10509-019-3532-1.
- [18] H. Jing, Z. Du, H. Li, H. Wang, J. He, C. Huo, Study on the reachable domain of earth–moon transfer orbits with terminal constraints in the cr3bp, *Acta Astronaut.* (2026). doi:10.1016/j.actaastro.2026.03.046.
- [19] E. A. Belbruno, J. K. Miller, Sun-perturbed earth-to-moon transfers with ballistic capture, *J. Guid. Control Dyn.* 16 (4) (1993) 770–775. doi:10.2514/3.21079.
- [20] C. Wang, W. Liu, Y. Gao, Low-energy earth–moon transfer autonomous guidance considering high-fidelity orbital dynamics, *Astrodynamics* 8 (4) (2024) 689–701. doi:10.1007/s42064-024-0211-y.
- [21] C. T. Campana, F. Topputo, Ephemeris refinement of low-energy earth-moon transfers via an astrodynamics model chain, *Acta Astronaut.* 232 (2025) 271–282. doi:10.1016/j.actaastro.2025.03.010.
- [22] W. S. Koon, M. W. Lo, J. E. Marsden, S. D. Ross, Low energy transfer to the moon, *Celest. Mech. Dyn. Astron.* 81 (1-2) (2001) 63–73. doi:10.1023/A:1013359120468.
- [23] S. Fu, D. Wu, P. Shi, S. Gong, Four-body transit-orbit classification combining lagrangian coherent structures with data mining, *J. Guid. Control Dyn.* (2025) 1–20doi:10.2514/1.G008681.

- [24] N. Hiraiwa, M. Bando, Y. Sato, S. Hokamoto, Design of low-energy transfers in cislunar space using sequences of lobe dynamics, *Acta Astronaut.* (2026). doi:10.1016/j.actaastro.2026.05.032.
- [25] S. Fu, Z. Xu, D. Wu, S. Gong, Deep neural network-based high-precision identification of weak stability boundary structures, *IEEE Trans. Aerosp. Electron. Syst.* (2026). doi:10.1109/TAES.2026.3668754.
- [26] K. Oshima, F. Topputo, S. Campagnola, T. Yanao, Analysis of medium-energy transfers to the moon, *Celest. Mech. Dyn. Astron.* 127 (3) (2017) 285–300. doi:10.1007/s10569-016-9727-7.
- [27] P. Dutt, A review of low-energy transfers, *Astrophys. Space Sci.* 363 (12) (2018) 253. doi:10.1007/s10509-018-3461-4.
- [28] C. T. Campana, F. Topputo, Clustering of earth-moon transfers in sun-perturbed environment, in: *2024 IEEE Congress on Evolutionary Computation (CEC)*, IEEE, 2024, pp. 1–8. doi:10.1109/CEC60901.2024.10611828.
- [29] A. Pinelli, Neural network applications to bi-impulsive earth-moon transfers in a four-body model, Master's thesis, Politecnico di Milano (2023).
- [30] W. Litteri, A. Francisco Gil, M. Vasile, V. Rodriguez-Fernandez, D. Camacho, Generation of periodic orbits in the restricted three-body problem with a variational autoencoder, *Celest. Mech. Dyn. Astron.* 138 (2026) 25. doi:10.1007/s10569-026-10299-x.
- [31] L. Dinh, J. Sohl-Dickstein, S. Bengio, Density estimation using real nvp, *arXiv preprint arXiv:1605.08803* (2016). doi:10.48550/arXiv.1605.08803.
- [32] J. Graebner, R. Beeson, Global search for optimal low thrust spacecraft trajectories using diffusion models and the indirect method, *J. Astronaut. Sci.* 72 (6) (2025) 62. doi:10.1007/s40295-025-00535-1.
- [33] T. Presser, A. Dasgupta, D. Erwin, A. Oberai, Diffusion models for generating ballistic spacecraft trajectories, *arXiv preprint arXiv:2405.11738* (2024). doi:10.48550/arXiv.2405.11738.
- [34] S. Fu, D. Wu, S. Gong, Discontinuous behavior of time-of-flight distribution for bi-impulsive earth-moon transfers in the three-body model, *arXiv preprint arXiv:2510.26567* (2025).
- [35] J. Ho, A. Jain, P. Abbeel, Denoising diffusion probabilistic models, in: H. Larochelle, M. Ranzato, R. Hadsell, M. Balcan, H. Lin (Eds.), *Advances in Neural Information Processing Systems*, Vol. 33, Curran Associates, Inc., 2020, pp. 6840–6851.
- [36] A. Vaswani, N. Shazeer, N. Parmar, J. Uszkoreit, L. Jones, A. N. Gomez, L. u. Kaiser, I. Polosukhin, Attention is all you need, in: I. Guyon, U. V. Luxburg, S. Bengio, H. Wallach, R. Fergus, S. Vishwanathan, R. Garnett (Eds.), *Advances in Neural Information Processing Systems*, Vol. 30, Curran Associates, Inc., 2017.

CRediT authorship contribution statement

Shuyue Fu: Data curation, Formal analysis, Methodology, Software, Writing - Original draft preparation, Writing - review & editing. **Wenxuan Zhang:** Methodology, Formal analysis, Writing - review & editing. **Di Wu:** Conceptualization, Methodology, Software, Writing - review & editing. **Shengping Gong:** Conceptualization, Funding acquisition, Writing - review & editing. **Peng Shi:** Methodology, Formal analysis, Writing - review & editing.